AGU PUBLICATIONS

JGR

Journal of Geophysical Research: Space Physics

RESEARCH ARTICLE
10.1002/2014JA019861

Key Points:
- Dust ringing effects are detected by RPWS after some dust impacts
- The ringing frequency is consistent with the local plasma frequency
- Dust ringing events provide an independent measurement of the electron density

Correspondence to:
S.-Y. Ye,
shengyi-ye@uiowa.edu

Citation:
Ye, S.-Y., D. A. Gurnett, W. S. Kurth, T. F. Averkamp, M. Morooka, S. Sakai, and J.-E. Wahlund (2014), Electron density inside Enceladus plume inferred from plasma oscillations excited by dust impacts, *J. Geophys. Res. Space Physics*, *119*, 3373–3380, doi:10.1002/2014JA019861.

Received 6 FEB 2014
Accepted 19 APR 2014
Accepted article online 24 APR 2014
Published online 7 MAY 2014

Electron density inside Enceladus plume inferred from plasma oscillations excited by dust impacts

S.-Y. Ye[1], D. A. Gurnett[1], W. S. Kurth[1], T. F. Averkamp[1], M. Morooka[2], S. Sakai[3], and J.-E. Wahlund[4]

[1]Department of Physics and Astronomy, University of Iowa, Iowa City, Iowa, USA, [2]LASP, University of Colorado at Boulder, Boulder, Colorado, USA, [3]Department of Cosmosciences, Hokkaido University, Sapporo, Japan, [4]Swedish Institute of Space Physics, Uppsala, Sweden

Abstract Enceladus' southern plume is one of the major discoveries of the Cassini mission. The water neutrals and water ice particles (dust) ejected by the cryovolcanic activity populate Saturn's E ring and the neutral torus, and they interact with the plasma environment of Saturn's magnetosphere. The plasma neutrality inside Enceladus' plume has been shown by the Langmuir probe measurement to be modified by the presence of the dust particles. We present an independent method of determining the electron density inside the plume. Sometimes, after dust impacts, plasma oscillations (ringing) were detected by the Cassini Radio and Plasma Wave Science instrument. The frequencies of these oscillations have been shown to be consistent with the local plasma frequency, thus providing a measurement of the local electron density.

1. Introduction

In 2005, the Cassini magnetometer detected a deflection of the magnetic field near Enceladus, indicating the existence of an atmospheric plume near the south pole of the moon [*Dougherty et al.*, 2006], which was confirmed by optical measurements by the imaging science subsystem [*Porco et al.*, 2006]. The plume consists of both water group neutrals [*Waite et al.*, 2006; *Hansen et al.*, 2006] and water ice particles (dust) [*Spahn et al.*, 2006; *Schmidt et al.*, 2008], which supply Saturn's plasma torus and E ring.

The properties of the dust particles ejected by Enceladus are measured by various instruments on board Cassini. The Cosmic Dust Analyzer is designed to measure the size, speed, composition, potential, and flux of micron-sized dust particles [*Srama et al.*, 2004, 2006; *Kempf et al.*, 2006; *Kempf*, 2008; *Kempf et al.*, 2008]. The Radio and Plasma Wave Science (RPWS) experiment detected micrometer size dust particles during the Saturn orbit insertion [*Wang et al.*, 2006] and E ring crossings in 2005 [*Kurth et al.*, 2006]. The RPWS Langmuir probe found large differences between ion and electron densities in the vicinity of Enceladus and ion velocities lower than the corotation speed [*Wahlund et al.*, 2009; *Yaroshenko et al.*, 2009; *Shafiq et al.*, 2011; *Morooka et al.*, 2011]. These authors argued that the dust particles are responsible for the absorption of electrons and the slowing down of the corotating ions. Nanometer size particles are detected by the Cassini Plasma Spectrometer (CAPS) ion mass and electron spectrometers [*Jones et al.*, 2009; *Hill et al.*, 2012]. The nanoparticles appear as high-energy ions and electrons in the CAPS spectrometers. The number density of these nanoparticles is much larger than that of micron-sized dust particles, and they could be responsible for most of the electron absorption inside the plume [*Hill et al.*, 2012].

Measurements of the electron density in the vicinity of Enceladus have been reliant on the RPWS experiment, which involves two methods, Langmuir probe [*Morooka et al.*, 2009] and the analysis of upper hybrid resonance [*Persoon et al.*, 2009]. The Langmuir probe uses a sweeping voltage, and the ion and electron density can be inferred from the current balance. It is found that in the Enceladus plume, the electron density is significantly lower than the ion density, suggesting that the majority of electrons are attached to submicron size dust particles [*Shafiq et al.*, 2011; *Morooka et al.*, 2011]. The electron density can also be derived from the upper hybrid frequency $f_{uh} = \sqrt{f_{ce}^2 + f_{pe}^2}$, given the local electron cyclotron frequency f_{ce}. The plasma frequency $f_{pe} = 9000\sqrt{n_e}$ Hz, where n_e is the electron density in cm^{-3}. However, the upper hybrid resonance frequency is hard to identify when the spacecraft is inside the plume, where the intense broadband bursty emission generated by dust impacts lowers the gain of the receiver and overwhelms any other signal. In this paper, we present a new and independent method of measuring the electron density (within a range from 1 to 100 cm^{-3}) inside the plume based on the dust impact-induced voltage ringing

recorded by the RPWS wideband receiver (WBR). Similar meteor-spacecraft impact-induced plasma oscillations, a possible cause of many spacecraft anomalies, have been discussed in the theoretical work by *Close et al*. [2010]. The ringing frequency is assumed to be at the local plasma frequency. The electron density derived from this method will be compared with the RPWS Langmuir probe measurement and the density inferred from the upper hybrid band, when visible. We will also briefly discuss the occurrence condition and generation mechanism of the dust impact ringing phenomenon.

2. Instrument Description

The RPWS WBR is designed to measure high-resolution electric and magnetic field waveforms in either a 10 kHz or 80 kHz bandwidth [*Gurnett et al*., 2004]. The WBR processes signals from a single sensor (selected from the E_x dipole, E_u, E_v, E_w monopole electric antenna, B_x magnetic antenna, or Langmuir probe). The magnetic search coil is not sensitive to high-enough frequencies to measure the dust ringing effect. For the data presented in this paper, the WBR was connected to the E_x electric dipole antenna. The WBR has an instantaneous dynamic range of 48 dB. In order to accommodate the large dynamic range of the input signals, an amplifier with a set of automatically selected gain levels is used to amplify the signal to the proper level in steps of 10 dB over a range of 0–70 dB, providing an over 100 dB dynamic range for the WBR. The sampling rate is 27,777 samples/s for the 10 kHz mode and 222,222 samples/s for the 80 kHz mode. The receiver operates in burst mode with 1536 samples (~ 7 ms) in each snapshot for the 80 kHz mode data presented in this paper. Note that for the 80 kHz mode used in this paper, the Nyquist frequency is 111.1 kHz; an antialiasing filter starts to roll-off at 75 kHz, and signals are not typically observed above about 90 kHz.

The RPWS Langmuir probe is designed to provide in situ information of the ambient plasma [*Wahlund et al*., 2005]. The probe is a 50 mm diameter sphere of titanium with a titanium nitride coating. When deployed, the probe is 1.5 m from the nearest spacecraft surface. The probe bias voltage is swept from −32 to +32 V relative to the spacecraft in less than 1 s. Depending on the probe potential, electrons and ions from the ambient plasma will be attracted or repelled, and for each of the 256 voltage steps the current to the probe is measured. The temperatures and the number densities of the electrons and ions in the ambient plasma can be estimated from the voltage-current characteristics. The errors in the fitted electron temperature and number density are estimated to be less than 20% [*Gustafsson and Wahlund*, 2010].

3. Dust Impact Ringing Effect

When a dust particle impacts the spacecraft, the kinetic energy of the collision vaporizes the particle and part of the spacecraft surface material [*Gurnett et al*., 1983; *Meyer-Vernet*, 1985]. The impacting charges are collected by the spacecraft body or the antenna, resulting in a voltage pulse detected by the receiver [*Gurnett et al*., 1987; *Tsintikidis et al*., 1994; *Oberc*, 1996; *Pantellini et al*., 2012; *Zaslavsky et al*., 2012; *Lee et al*., 2012, 2013]. A typical dust impact-induced voltage pulse is shown in Figure 1. The dust ringing effect, characterized as periodic voltage oscillations after the initial voltage pulse, can sometimes be observed after a dust impact. A sample waveform of the dust impact ringing effect is shown in Figure 1 in comparison with the normal dust impact. The ringing effect typically lasts around 1 ms.

Because of the frequencies involved, we only use the 80 kHz mode of the WBR instrument in this study. An algorithm is developed to identify the dust ringing events and compute the ringing frequency (Figure 2). First, a short period of the waveform (50 data points) following the initial voltage jump is detrended, by subtracting a moving average (10 data point window). The voltage oscillation is identified as the zero crossings in the detrended data (We require a minimum of five zero crossings with minimum amplitude of two digitizing steps within the 50 point period.). The digitizing step is used because the different gain levels effectively redefine the minimum amplitude in an absolute sense. The length of the identification period and the required number of zero crossings places a lower limit on the detected frequency at around 10 kHz. The antialiasing filter places an upper limit of about 90 kHz on the detectable frequency range. Hence, the effective range of the electron density that can be determined by the dust ringing method is about 1 to 100 cm^{-3}. Note that all of the dust ringing electron densities shown in the figures below fall in this range. The dominant oscillation (ringing) frequency is found by the fast Fourier transform (FFT) over the same 50-point data window. The spectral power of the oscillation is compared with the peak FFT power of the data period

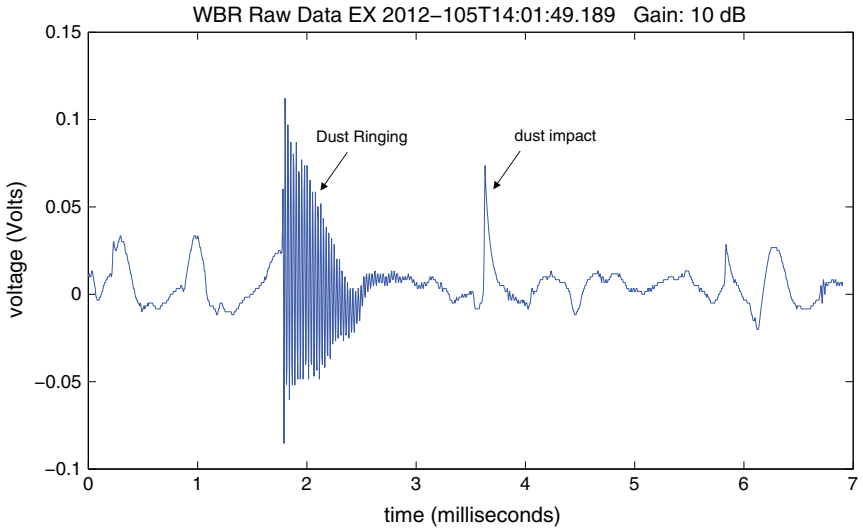

Figure 1. A sample waveform snapshot of WBR showing the dust ringing effect (voltage oscillations after the initial voltage pulse) in comparison with a normal dust impact.

(50 data points) just prior to the dust impact. The spectral power of the current period oscillation has to be 3 times larger than the previous period for it to be qualified as a dust impact ringing event.

Figure 3 shows the ringing frequencies calculated from the ringing events observed during the E03 flyby. The electric field power spectrogram shows the upper hybrid resonance (narrowband emission in the spectrogram) observed during the flyby. The upper hybrid resonance frequencies digitized from the wideband data are plotted as red dots in the second panel in comparison to the ringing frequencies. Third and fourth panels show the occurrence ratio of the dust ringing events and the gain level of WBR. The dust ringing frequency follows the trend of the upper hybrid frequency where they are both observable outside the plume. At Enceladus the electron cyclotron frequency f_{ce} is around 10 kHz; therefore, the upper hybrid frequency f_{uh} is fairly close to the plasma frequency f_{pe}. Inside the Enceladus plume, it is difficult to identify the upper hybrid resonance frequency due to the intense broadband bursts caused by the dust impacts and the resulting lower gain of the receiver. Therefore, the Langmuir probe electron density data are needed to compare with the electron density derived from the ringing frequencies.

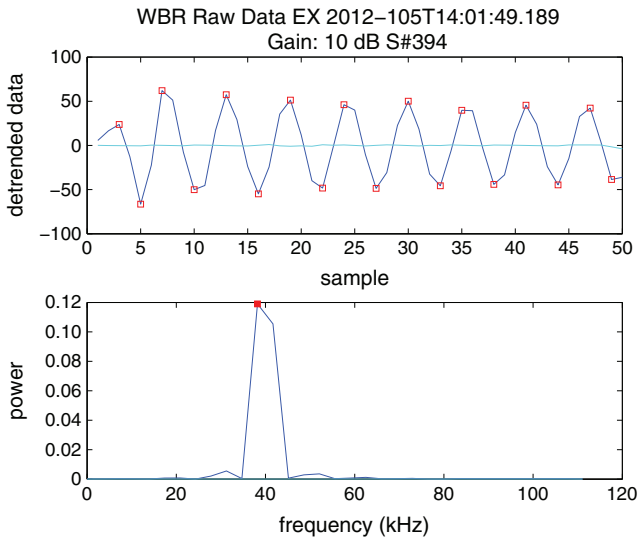

Figure 2. Fast Fourier transform of the detrended dust ringing waveform. The waveform and spectrum of the ringing event (blue) are compared with those of the 50 sample periods before the dust impact (teal). The hollow red squares are the local maxima and minima that exceed the amplitude threshold of two data points. The solid red square marks the peak of the ringing spectral power at ~38 kHz.

4. Electron Density Profile Inferred From Dust Impact Ringing Frequencies

Figure 4 shows the electron density profile derived from the dust impact ringing frequencies measured during the E03–E06 flybys. In the E03 flyby, the dropout in the electron density before the closest approach is also observed in the Langmuir probe observations presented by *Morooka et al.* [2011]. The electron density dropout is due to the

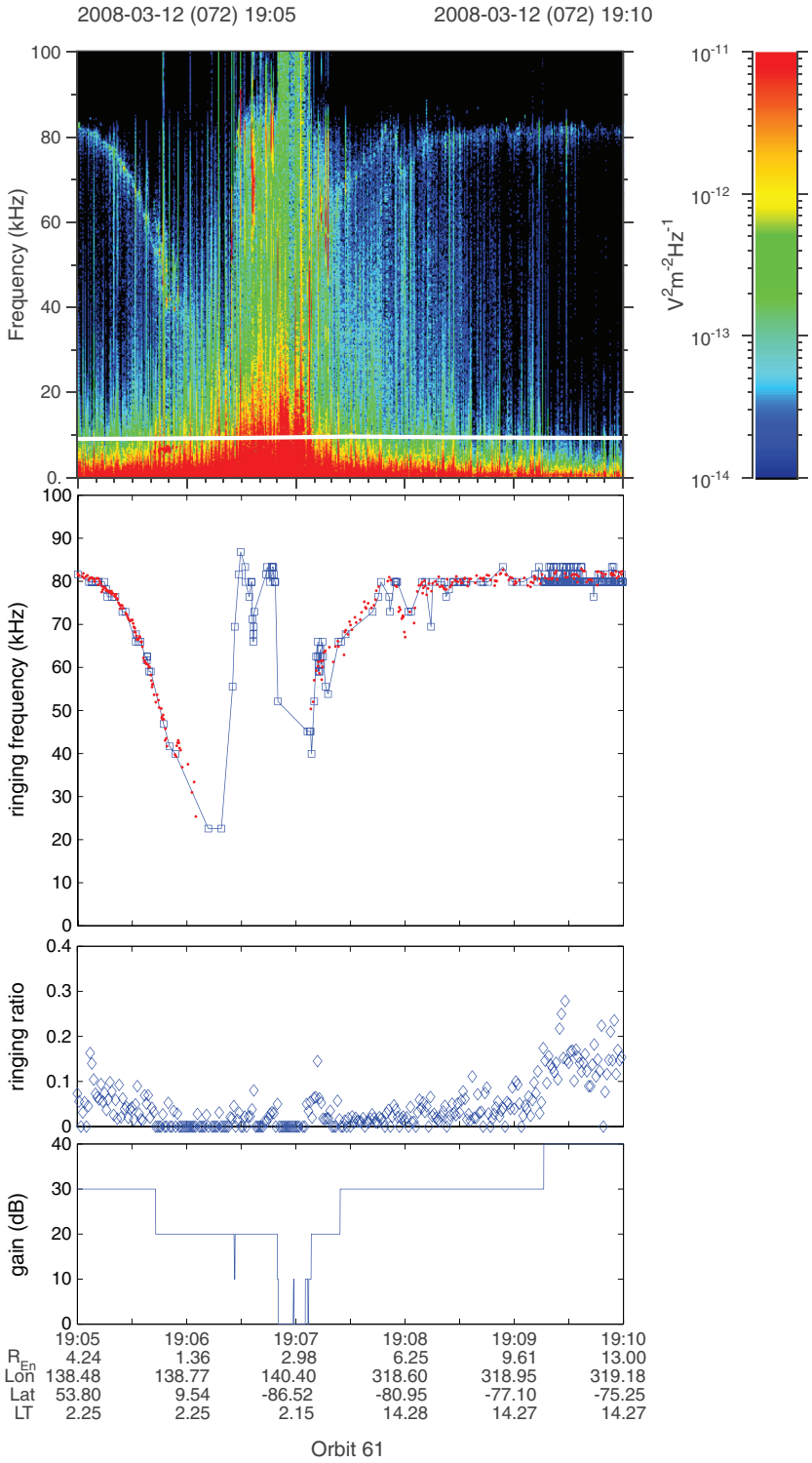

Figure 3. First and second panels show electric field power spectrogram and dust ringing frequency measured during the E03 flyby. The upper hybrid resonance frequencies digitized from the wideband data are plotted as red dots in comparison to the ringing frequencies (blue squares). Third and fourth panels show the occurrence ratio of the dust ringing events relative to all dust impacts and the gain level of the wideband receiver.

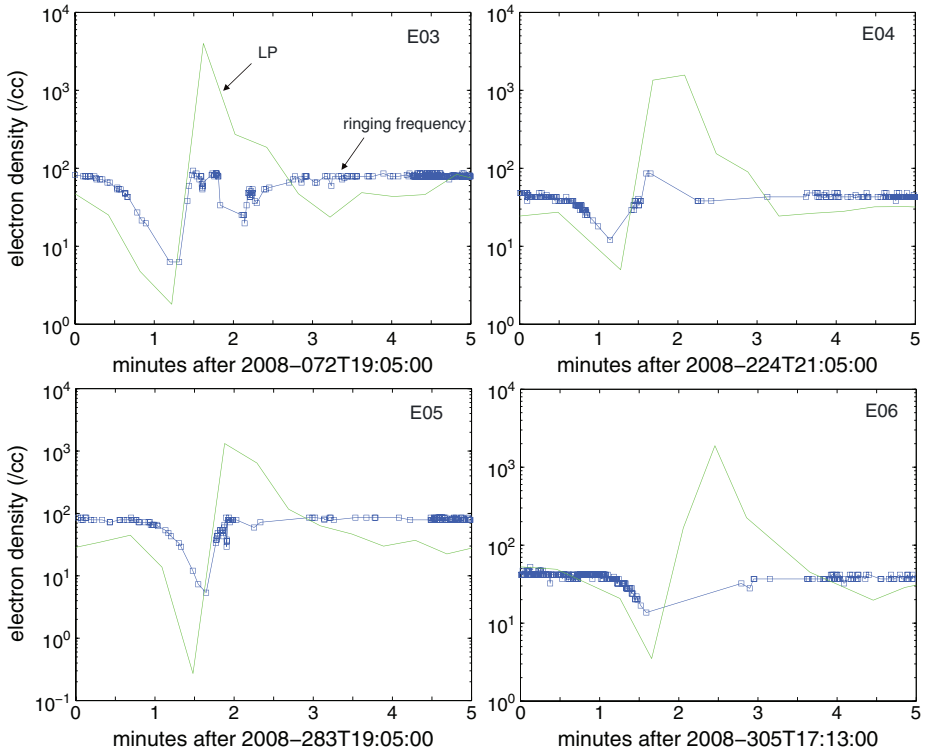

Figure 4. E03, E04, E05, and E06 flybys. Blue: electron densities derived from dust ringing frequencies. Green: electron densities measured by the Langmuir probe.

absorption of electrons by the dust particles [*Farrell et al*., 2009; *Hill et al*., 2012]. The electron density increases sharply inside the plume, where new plasma is generated from ionization of the materials ejected from the south pole of Enceladus. The Langmuir probe observations show that the electron density is ~ 4000 cm^{-3}, which corresponds to plasma frequencies (~ 500 kHz) well above the Nyquist frequency of the WBR (111.1 kHz) and the roll-off frequency of the antialiasing filter. So the plasma frequencies corresponding to the Langmuir probe electron density measurements near the center of the plume are beyond the detection limit of the dust ringing method. Note that the upper limit of the electron density measurement via dust ringing is ~ 100 cm^{-3} as imposed by the antialiasing filter. In contrast to the sharp increase in electron density measured by the Langmuir probe, the ringing frequencies dipped below the upper detection limit (100 cm^{-3}). The dipping of the ringing frequencies is not a result of aliasing because the frequencies would mirror at the Nyquist frequency (111.1 kHz) instead of around 80 kHz. The discrepancy between the Langmuir probe and the ringing methods in this region remains unresolved. Nonetheless, before the detection limit of the WBR is reached, the electron densities measured by the two methods agree pretty well. The electron density profile derived from the dust ringing frequencies clearly shows the electron depletion before and after Cassini flew through the plume and the electron density enhancement near the center of the plume. The E04, E05, and E06 flybys had similar high-inclination trajectories as that of E03. Similar electron density depletion on the perimeter of the plume and electron density enhancement near the center of the plume was observed during these flybys. Fewer dust ringing events were observed during the E06 flyby, so the inferred electron density profile inside the plume does not have enough resolution to resolve the electron density enhancement. One possible explanation for the lack of observations of dust ringing events inside the plume is that the actual ringing frequencies are above the detection limit of the WBR.

It is also noteworthy that the background electron density level near Enceladus varied from flyby to flyby, consistent with the longitudinal electron density modulation in the inner magnetosphere observed by *Gurnett et al*. [2007]. Langmuir probe measurements of the spacecraft potential, which can be approximated as the dust potential, during the Enceladus flybys varies with the SKR longitude, with the least negative potential measured where the E ring plasma is densest [*Morooka et al*., 2011]. The reduction in the negative

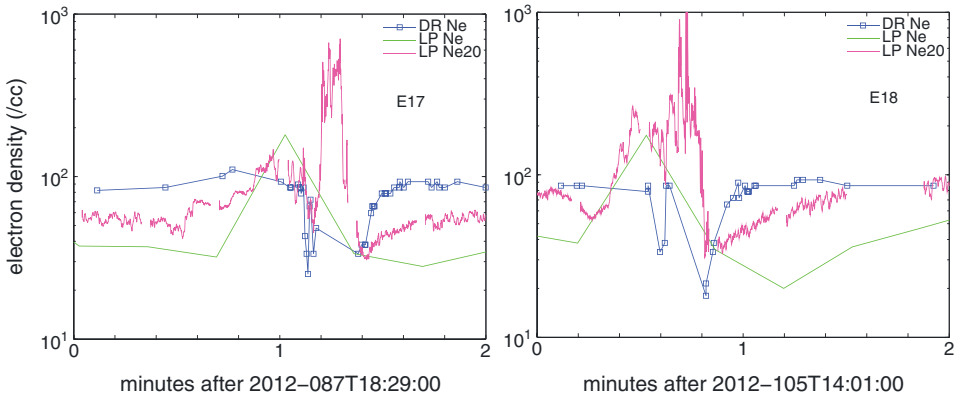

Figure 5. E17 and E18 flybys. Blue: electron densities derived from dust ringing frequencies. Green: electron densities measured by the Langmuir probe. Magenta: Langmuir probe 20 Hz electron densities, which is based on the sweep density measurement (green) and the relative density variations between sweeps.

potential of dust particles reduces their electrostatic grip on the ion population which leads to plasma outflow. It is proposed that the dust-plasma interaction in the E ring is the cause of the planetary spin-modulated dynamics of Saturn's magnetosphere.

The E17 and E18 flybys had horizontal trajectories that cut through the base of the Enceladus plume at an altitude of 1.3 R_E (Enceladus radius = 252 km). Figure 5 shows the electron density derived from ringing frequencies detected during these flybys. For comparison, the electron density measured by the Langmuir probe is plotted in green. The Langmuir probe 20 Hz electron density data (based on the sweep data) are plotted in magenta, which shows the higher-resolution electron density structure of the plume. The electron density profiles generated from the dust ringing events are generally consistent with the Langmuir probe measurements where $f_{pe} < 90$ kHz. Note that the RPWS electron density measurement inside the plume is dependent on the occurrence of the dust ringing, so the spatial resolution of the electron density profile is highly variable. The electron density fine structures due to the multiple subplumes [*Porco et al.*, 2006; *Jones et al.*, 2009] could not be resolved by the electron density profiles inferred from the dust ringing events observed during these two flybys.

Note that near Enceladus, the electron densities derived from the dust impact ringing frequencies are 2–3 times higher than the electron densities inferred from the Langmuir probe sweeps. Figure 4 of *Morooka et al.* [2011] shows that the Langmuir probe electron density and the upper hybrid frequency-derived electron density agree pretty well except when Cassini is within a couple of Enceladus radii of the moon. It appears that the change of plasma properties near the moon could affect the consistency between the electron densities measured by the two methods. One possibility is the increase of electron temperature near the moon. Due to the fact that the energy limit of Langmuir probe for electron density measurement is around 8 eV, the high-energy tail of the electron distribution is not measured by the Langmuir probe. As a result, the electron density inferred from the Langmuir probe will be lower than the actual electron density [*Gustafsson and Wahlund*, 2010].

5. Discussion

The dust impact ringing events detected during the Enceladus flybys provide an independent method of measuring the electron density (within the range from 1 to 100 cm^{-3}) inside the plume, which is previously only measured by the RPWS Langmuir probe. The electron density is a crucial parameter for modeling the Enceladus plume and its interaction with the plasma environment of Saturn [*Jia et al.*, 2010; *Kriegel et al.*, 2011; *Simon et al.*, 2011; *Farrell et al.*, 2012; *Omidi et al.*, 2012]. The knowledge of the electron and ion densities helps to constrain the dust size distributions measured by different instruments during the Enceladus flybys and E ring crossings [*Yaroshenko et al.*, 2009; *Shafiq et al.*, 2011; *Morooka et al.*, 2011; *Hill et al.*, 2012]. An accurate electron density also helps to understand the dusty plasma dynamics in the

vicinity of Enceladus, which serves as a natural laboratory for studying the dust-plasma interaction [*Morooka et al*., 2011; *Hsu et al*., 2012, 2013].

Close et al. [2010] put forth a possible mechanism for the generation of the ringing effect. They proposed that the expanding ion cloud accelerates the ambient electrons through the ambipolar electric field, causing electron plasma oscillations. It is also possible that the electrons from the impact plasma constitute a fast beam relative to the background plasma, which will excite Langmuir waves through the "bump-on-tail" instability, much like the way fast electrons from solar flares excite Langmuir waves in the solar wind [*Gurnett and Frank*, 1975; *Gurnett et al*., 1978].

The occurrence condition of the dust ringing events is still not clear, as most of the time voltage oscillations are not observed during the relaxation phase of the dust impacts (e.g., the nonringing dust impact in Figure 1). Statistics show that the percentage of occurrence of the ringing effect is between 0 and 30%, with more ringing events observed at higher gain levels (Figure 3, third and fourth panels). The ratio of the cross-sectional areas between the RPWS dipole antenna and the spacecraft body is on the order of 1 to 10. Due to the common mode rejection of the dipole mode, the impacts at locations relatively symmetric to the dipole antenna would not be strong enough to be detected, which means the effective area should be somewhat less than the cross section of the spacecraft body. As a result, the effective area of the electric dipole antenna could be as large as 30% of the effective area of the spacecraft body in the dipole mode. So it is plausible that the ringing events occur only when dust particles directly impact the electric antenna. Why dust ringing should be excited by direct impacts of dust particles on the antenna is still not understood.

6. Conclusion

We have found a new and independent method of measuring the electron density (within the range from 1 to 100 cm^{-3}) in heavily dust laden environments like the Enceladus plume. The ringing frequency of the voltage oscillations observed immediately after some dust impacts by the RPWS WBR is shown to be consistent with the local plasma frequency. Comparison of the electron density profile derived from the dust impact ringing frequencies with densities inferred from the upper hybrid band and the Langmuir probe shows general agreement between the three methods. In the vicinity of Enceladus, the electron density inferred from the Langmuir probe observations is 2–3 times lower than that derived from the dust ringing frequency. The underestimation could be due to the fact that the Langmuir probe is not sensitive to hot electrons above 8 eV. The percentage of occurrence of the dust ringing events is roughly consistent with direct impact on the electric antenna based on the relative cross-sectional area of the antenna versus the spacecraft body. The generation mechanism is briefly discussed. We propose excitation of Langmuir waves by the electron beams from the impact plasma via the bump-on-tail instability as the generation mechanism of the dust impact ringing phenomenon.

Acknowledgments

This research was supported by NASA through contract 1415150 with the Jet Propulsion Laboratory. The Swedish National Space Board (SNSB) supports the RPWS/ LP instrument on board Cassini. This work was also supported by Japan Society for the Promotion Science (JSPS). The data used in this study are available through the Planetary Data System or from the authors.

Michael Balikhin thanks Scott Boardsen and Paul J. Kellogg for their assistance in evaluating this paper.

References

Close, S., P. Colestock, L. Cox, M. Kelley, and N. Lee (2010), Electromagnetic pulses generated by meteoroid impacts on spacecraft, *J. Geophys. Res.*, *115*, A12328, doi:10.1029/2010JA015921.

Dougherty, M. K., K. K. Khurana, F. M. Neubauer, C. T. Russell, J. Saur, J. S. Leisner, and M. Burton (2006), Identification of a dynamic atmosphere at Enceladus with the Cassini magnetometer, *Science*, *311*, 1406–1409.

Farrell, W. M., W. S. Kurth, D. A. Gurnett, R. E. Johnson, M. L. Kaiser, J.-E. Wahlund, and J. H. Waite Jr. (2009), Electron density dropout near Enceladus in the context of water-vapor and water-ice, *Geophys. Res. Lett.*, *36*, L10203, doi:10.1029/2008GL037108.

Farrell, W. M., J.-E. Wahlund, M. W. Morooka, D. A. Gurnett, W. S. Kurth, and R. J. MacDowall (2012), The electromagnetic pickup of submicron-sized dust above Enceladus's northern hemisphere, *Icarus*, *219*, 498–501.

Gurnett, D. A., R. R. Anderson, F. L. Scarf, and W. S. Kurth (1978), The heliocentric radial variation of plasma oscillations associated with type III radio bursts, *J. Geophys. Res.*, *83*, 4147–4152, doi:10.1029/JA083iA09p04147.

Gurnett, D. A., and L. A. Frank (1975), Electron plasma oscillations associated with type III radio emissions and solar electrons, *Sol. Phys.*, *45*, 477–493.

Gurnett, D. A., E. Grün, D. Gallagher, W. S. Kurth, and F. L. Scarf (1983), Micron-sized particles detected near Saturn by the Voyager plasma wave instrument, *Icarus*, *53*, 236–254.

Gurnett, D. A., W. S. Kurth, F. L. Scarf, J. A. Burns, J. N. Cuzzi, and E. Grün (1987), Micron-sized particle impacts detected near Uranus by the Voyager 2 plasma wave instrument, *J. Geophys. Res.*, *92*, 14,959–14,968, doi:10.1029/JA092iA13p14959.

Gurnett, D. A., et al. (2004), The Cassini radio and plasma wave science investigation, *Space Sci. Rev.*, *114*, 395–463.

Gurnett, D. A., A. M. Persoon, W. S. Kurth, J. B. Groene, T. F. Averkamp, M. K. Dougherty, and D. J. Southwood (2007), The variable rotation period of the inner region of Saturn's plasma disk, *Science*, *316*, 442.

Gustafsson, G., and J. E. Wahlund (2010), Electron temperatures in Saturn's plasma disc, *Planet. Space Sci.*, *58*(7–8), 1018–1025, doi:10.1016/j.pss.2010.03.007.

Hansen, C. J., L. Esposito, A. I. F. Stewart, J. Colwell, A. Hendrix, W. Pryor, D. Shemansky, and R. West (2006), Enceladus' water vapor plume, *Science*, *311*, 1422–1425.
Hill, T. W., et al. (2012), Charged nanograins in the Enceladus plume, *J. Geophys. Res.*, *117*, A05209, doi:10.1029/2011JA017218.
Hsu, H.-W., M. Horányi, S. Kempf, and E. Grün (2012), Spacecraft charging near Enceladus, *Geophys. Res. Lett.*, *39*, L06108, doi:10.1029/2012GL050999.
Hsu, H.-W., M. Horanyi, and S. Kempf (2013), Dust and spacecraft charging in Saturn's E ring, *Earth Planets Space*, *65*, 149–156.
Jia, Y.-D., C. T. Russell, K. K. Khurana, Y. J. Ma, W. Kurth, and T. I. Gombosi (2010), Interaction of Saturn's magnetosphere and its moons: 3. Time variation of the Enceladus plume, *J. Geophys. Res.*, *115*, 13, doi:10.1029/2010ja015534.
Jones, G. H., et al. (2009), Fine jet structure of electrically charged grains in Enceladus's plume, *Geophys. Res. Lett.*, *36*, L16204, doi:10.1029/2009GL038284.
Kempf, S., et al. (2006), The electrostatic potential of E ring particles, *Planet. Space Sci.*, *54*, 999.
Kempf, S. (2008), Interpretation of high rate dust measurements with the Cassini dust detector CDA, *Planet. Space Sci.*, *56*, 378.
Kempf, S., U. Beckmann, G. Klostermeyer, F. Postberg, R. Srama, T. Economou, J. Schmidt, F. M. Spahn, and E. Grün (2008), The E ring in the vicinity of Enceladus I. Spatial distribution and properties of the ring particles, *Icarus*, *193*, 420–437.
Kriegel, H., S. Simon, U. Motschmann, J. Saur, F. M. Neubauer, A. M. Persoon, M. K. Daugherty, and D. A. Gurnett (2011), Influence of negatively charged plume grains on the structure of Enceladus' Alfvén wings: Hybrid simulations versus Cassini Magnetometer data, *J. Geophys. Res.*, *116*, A10223, doi:10.1029/2011JA016842.
Kurth, W. S., T. F. Averkamp, D. A. Gurnett, and Z. Wang (2006), Cassini RPWS observations of dust in Saturn's E ring, *Planet. Space Sci.*, *54*, 988–998.
Lee, N., et al. (2012), Measurements of freely-expanding plasma from hypervelocity impacts, *Int. J. Impact Eng.*, *44*, 40–49.
Lee, N., S. Close, A. Goel, D. Lauben, I. Linscott, T. Johnson, D. Strauss, S. Bugiel, A. Mocker, and R. Srama (2013), Theory and experiments characterizing hypervelocity impact plasmas on biased spacecraft materials, *Phys. Plasmas*, *20*, 032901.
Meyer-Vernet, N. (1985), Comet Giacobini-Zinner diagnosis from radio measurements, *Adv. Space Res.*, *5*, 37–46.
Morooka, M. W., et al. (2009), The electron density of Saturn's magnetosphere, *Ann. Geophys.*, *27*, 2971–2991.
Morooka, M. W., J.-E. Wahlund, A. I. Eriksson, W. M. Farrell, D. A. Gurnett, W. S. Kurth, A. M. Persoon, M. Shafiq, M. André, and M. Holmberg (2011), Dusty plasma in the vicinity of Enceladus, *J. Geophys. Res.*, *116*, A12221, doi:10.1029/2012JA017606.
Oberc, P. (1996), Electric antenna as a dust detector, *Adv. Space Res.*, *17*, 105–110.
Omidi, N., R. L. Taker, T. Averkamp, D. A. Gurnett, W. S. Kurth, and Z. Wang (2012), Flow stagnation at Enceladus: The effects of neutral gas and charged dust, *J. Geophys. Res.*, *117*, A06230, doi:10.1029/2011JA017488.
Pantellini, F., S. Belheouane, N. Meyer-Vernet, and A. Zaslavsky (2012), Nano dust impacts on spacecraft and boom antenna charging, *Astrophys. Space Sci.*, *341*, 309–314.
Persoon, A. M., et al. (2009), A diffusive equilibrium model for the plasma density in Saturn's magnetosphere, *J. Geophys. Res.*, *114*, A04211, doi:10.1029/2008JA013912.
Porco, C. C., et al. (2006), Cassini observes the active south pole of Enceladus, *Science*, *311*, 1393–1401.
Schmidt, J., N. Brilliantov, F. Spahn, and S. Kempf (2008), Slow dust in Enceladus' plume from condensation and wall collisions in tiger fracture, *Nature*, *451*, 685–688.
Shafiq, M., J.-E. Wahlund, M. W. Morooka, W. S. Kurth, and W. M. Farrell (2011), Characteristics of the dust-plasma interaction near Enceladus' south pole, *Planet. Space Sci.*, *59*, 17–25.
Simon, S., J. Saur, H. Kriegel, F. M. Neubauer, U. Motschmann, and M. K. Daugherty (2011), Influence of negative charged plume grains and hemisphere coupling currents on the structure of Enceladus' Alfvén wings: Analytical modeling of Cassini magnetometer observations, *J. Geophys. Res.*, *116*, A04221, doi:10.1029/2010JA016338.
Spahn, F., et al. (2006), Cassini dust measurements at Enceladus and implications for the origin of the E ring, *Science*, *311*, 1416–1418.
Srama, R., et al. (2006), In situ dust measurements in the inner Saturnian system, *Planet. Space Sci.*, *54*, 967.
Srama, R., et al. (2004), The Cassini cosmic dust analyzer, *Space Sci. Rev.*, *114*, 465–518.
Tsintikidis, D., D. A. Gurnett, L. J. Granroth, S. C. Allendorf, and W. S. Kurth (1994), A revised analysis of micron-sized particle detected near Saturn by the Voyager 2 plasma wave instrument, *J. Geophys. Res.*, *99*(A2), 2261–2270, doi:10.1029/93JA02906.
Wahlund, J.-E., et al. (2005), The inner magnetosphere of Saturn: Cassini RPWS cold plasma result from the first encounter, *Geophys. Res. Lett.*, *32*, L20S09, doi:10.1029/2005GL022699.
Wahlund, J.-E., et al. (2009), Detection of dusty plasma near the E-ring of Saturn, *Planet. Space Sci.*, *57*, 1795–1806.
Waite, J. H., et al. (2006), Cassini ion and neutral mass spectrometer: Enceladus plume composition and structure, *Science*, *311*, 1419–1422.
Wang, Z., D. A. Gurnett, T. F. Averkamp, A. M. Persoon, and W. S. Kurth (2006), Characteristics of dust particles detected near Saturn's ring plane, *Planet. Space Sci.*, *54*, 957–966.
Yaroshenko, V. V., S. Ratynskaia, J. Olson, N. Brenning, J.-E. Wahlund, M. Morooka, W. S. Kurth, D. A. Gurnett, and G. E. Morfill (2009), Characteristics of charged dust inferred from the Cassini RPWS measurements in the vicinity of Enceladus, *Planet. Space Sci.*, *57*, 1807–1812.
Zaslavsky, A., et al. (2012), Interplanetary dust detection by radio antennas: Mass calibration and fluxes measured by STEREO/WAVES, *J. Geophys. Res.*, *117*, A05102, doi:10.1029/2011JA017480.